

Pulse generation in Yb-doped polarization-maintaining fiber laser by nonlinear polarization evolution

Cheng-Bin Liang(梁成斌), Yan-Rong Song(宋晏蓉), Zi-Kai Dong(董自凯), Yun-Feng Wu(吴云峰), Jin-Rong Tian(田金荣), Run-Qin Xu(徐润亲)

Citation: Chin. Phys. B . 2020, 29(7): 074206 . **doi:** 10.1088/1674-1056/ab8ac6
Journal homepage: http://cpb.iphy.ac.cn; http://iopscience.iop.org/cpb

What follows is a list of articles you may be interested in

$CsPbBr_3$ nanocrystal for mode-locking Tm-doped fiber laser

Yan Zhou(周延), Renli Zhang(张仁栗), Xia Li(李夏), Peiwen Kuan(关珮雯), Dongyu He(贺冬钰), Jingshan Hou(侯京山), Yufeng Liu(刘玉峰), Yongzheng Fang(房永征), Meisong Liao(廖梅松)

Chin. Phys. B . 2019, 28(9): 094203 . **doi:** 10.1088/1674-1056/ab327c

7.6-W diode-pumped femtosecond Yb: KGW laser

Yan-Fang Cao(曹艳芳), Xiang-Hao Meng(孟祥昊), Jun-Li Wang(王军利), Zhao-Hua Wang(王兆华), Meng-Yao Cheng(程梦尧), Jiang-Feng Zhu(朱江峰), Zhi-Yi Wei(魏志义)

Chin. Phys. B . 2019, 28(4): 044205 . **doi:** 10.1088/1674-1056/28/4/044205

Observation of stable bound soliton with dual-wavelength in a passively mode-locked Er-doped fiber laser

Yu Zheng(郑煜), Jin-Rong Tian(田金荣), Zi-Kai Dong(董自凯), Run-Qin Xu(徐润亲), Ke-Xuan Li(李克轩), Yan-Rong Song(宋晏蓉)

Chin. Phys. B . 2017, 26(7): 074212 . **doi:** 10.1088/1674-1056/26/7/074212

Tunable second harmonic generation from a Kerr-lens mode-locked Yb: $YCa_4O(BO_3)_3$ femtosecond laser

Zi-Ye Gao(高子叶), Jiang-Feng Zhu(朱江峰), Zheng-Mao Wu(吴正茂), Zhi-Yi Wei(魏志义), Hao-Hai Yu(于浩海), Huai-Jin Zhang(张怀金), Ji-Yang Wang(王继扬)

Chin. Phys. B . 2017, 26(4): 044202 . **doi:** 10.1088/1674-1056/26/4/044202

Two-dimensional materials for ultrafast lasers

Fengqiu Wang(王枫秋)

Chin. Phys. B . 2017, 26(3): 034202 . **doi:** 10.1088/1674-1056/26/3/034202

Pulse generation in Yb-doped polarization-maintaining fiber laser by nonlinear polarization evolution*

Cheng-Bin Liang(梁成斌)[1], Yan-Rong Song(宋晏蓉)[1,†], Zi-Kai Dong(董自凯)[1], Yun-Feng Wu(吴云峰)[1], Jin-Rong Tian(田金荣)[1], and Run-Qin Xu(徐润亲)[2]

[1] *College of Applied Sciences, Beijing University of Technology, Beijing* 100124, *China*
[2] *Institute of Automation, Chinese Academy of Sciences, Beijing* 100190, *China*

(Received 4 March 2020; revised manuscript received 6 April 2020; accepted manuscript online 18 April 2020)

We demonstrate a self-started, long-term stable polarization-maintaining mode-locked fiber laser based on the nonlinear polarization evolution technique. A polarized beam splitter is inserted into the cavity of the linear polarization-maintaining fiber laser to facilitate self-started mode-locking. Pulses with single pulse energy of 26.9 nJ and average output power of 73.9 mW are obtained at the pump power of 600 mW. The transmission characteristics of artificial saturable absorber used in this laser are analyzed theoretically, the influence of the half-wave plate state on mode-locking is discussed, and the mode-locking range is obtained, which is well consistent with the experimental results.

Keywords: polarization-maintaining, mode-locking, nonlinear polarization evolution

PACS: 42.55.Wd, 42.60.Fc, 42.81.Gs **DOI:** 10.1088/1674-1056/ab8ac6

1. Introduction

Mode locked all-normal-dispersion fiber lasers have been widely used in many fields due to their compactness and high pulse energy. Polarization-maintaining (PM) fiber lasers are a practicable solution to eliminating the environment-induced instabilities caused by thermal and mechanical perturbations. However, the mode locking of a PM fiber laser is difficult, which is in contrast with the mode locking of the laser without PM fiber. Typically there are three techniques to implement mode-locking in polarization-maintaining lasers. First one is the implementation of nonlinear optical loop mirror (NOLM)[1,2] or nonlinear amplifying loop mirror (NALM).[2,3] Second one is based on material saturable absorbers such as semiconductor saturable absorber mirror,[4] graphene,[5–7] or carbon nanotubes.[8–11] The third one is the application of nonlinear polarization evolution (NPE) technique to the PM fiber laser.[12]

For NPE-based PM mode locked fiber lasers, there are still three methods to realize mode-locking. The first one is to splice different PM fiber segments together with precise lengths and angles to compensate for group velocity mismatch (GVM) introduced by the strong linear birefringence.[13] Wang *et al.* proposed a cross-splicing method to compensate for all the birefringences of PM fibers, and obtained a pulse width of 11.7 ps, repetition frequency of 48.3 MHz and pulse energy of 2.1 nJ, respectively.[14] Zhou *et al.* inserted an NPE section based on three PM fiber segments into the laser to compensate for GVM and obtained pulses with a repetition frequency of 90.5 MHz, pulse width of 90 ps and pulse energy of 77 pJ, respectively.[15] However, the length of the PM fiber should be carefully controlled below one-eighth of the beat length of the PM fiber, which is difficult to realize.[16] The second method is to use Faraday rotator and Faraday mirror to automatically compensate for the GVM of the PM fibers. Zhou *et al.* demonstrated such a kind of laser to produce dissipative soliton (DS) pulses with pulse energy of 2.9 nJ and pulse width of 5.9 ps.[17] Peng *et al.* constructed a laser based on Faraday mirror to deliver the average power of 388 μW at 15.4-MHz repetition rate. The spectral width and pulse duration were 5.1 nm and 700 fs, respectively.[18] The third method is to combine the above two methods. Szczepanek *et al.* presented a PM NPE section based on three PM fiber segments and a Faraday mirror.[16] Based on this structure, mode locking was obtained in 2019.[19]

The aforementioned methods require at least one special angle splicing fiber, which is not easy to control in experiment. In this paper, a polarized beam splitter (PBS), instead of angle splicing or precisely matching the length of each fiber, is inserted into a linear PM fiber laser cavity to facilitate self-start mode-locking. Furthermore, the transmission characteristics of the artificial saturable absorber (ASA) can be tuned by rotating the PBS, and mode-locking is obtained easily. This is a simple and flexible design in contrast with common methods. A half-wave plate (HWP) is also used to facilitate mode-locking. To investigate the characteristics of the output pulses, different cavity lengths of 23 m, 38 m, and 99 m are used alternatively in this laser. The pulse energy of 26.9 nJ and average

*Project supported by the National Natural Science Foundation of China (Grant Nos. 61575011 and 61975003) and the Beijing Natural Science Foundation, China (Grant No. 4192015).

†Corresponding author. E-mail: yrsong@bjut.edu.cn

© 2020 Chinese Physical Society and IOP Publishing Ltd

power of 73.9 mW are obtained at the pump power of 600 mW. Finally, the numerical simulation is carried out to justify the mechanism of the mode locking.

2. Experimental setup and theoretical model

Figure 1 shows the experimental setup of the linear cavity PM mode-locked fiber laser based on NPE technology. The cavity is composed of a 35-cm PM Yb-doped fiber (PM-YSF-HI), a PM 980 fiber (group velocity dispersion of 26.7 ps·(nm·km)$^{-1}$@1030 nm), a PM wavelength division multiplexer (PM WDM), a Faraday rotator, an HWP, two collimators, two mirrors, and all of them operate at a center wavelength of 1030 nm. The type of the pigtail fibers of WDM and collimators are PM 980. The pump light from a 975-nm laser diode is coupled into a PM Yb-doped fiber through the PM WDM. The HWP is tilted at Brewster angle with respect to the beam direction. Three cavity lengths of 23 m, 38 m, and 99 m are used in experiment, respectively.

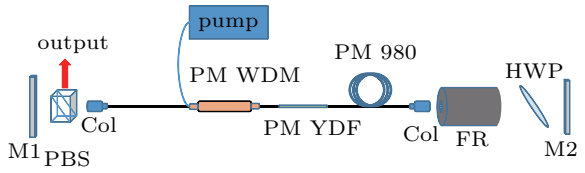


Fig. 1. Experimental setup of PM mode-locked fiber laser. PBS: olarization beam splitter; PM WDM: PM wavelength-division multiplexer; PM 980: PM 980 fiber; PM YDF: PM ytterbium-doped fiber; Col: PM collimator; HWP: half-wave plate; FR: Faraday rotator; M1: mirror; M2: end mirror.

Each element of the NPE laser will influence the saturable absorption of the laser, therefore, we consider the whole NPE structure as an ASA and establish a model to analyze the transmission characteristics of the ASA. Figure 2 shows the model of the ASA. The ASA can be equivalently simplified into five parts: end mirror, polarizer, PM fiber, Faraday rotator, and HWP. Here the polarizer represents the PBS in the linear cavity (in Fig. 1), θ is the angle of the transmission axis of the polarizer with respect to the x axis, α is the azimuth angle included between the plane of incidence and the main plane of HWP.[20]

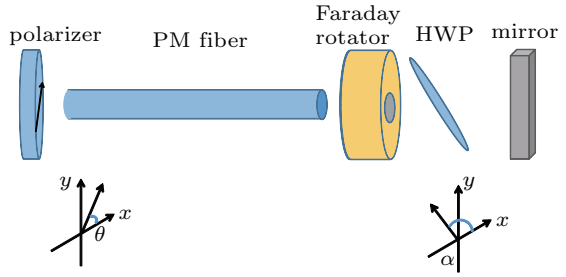


Fig. 2. Simplified theoretical model of ASA with x axis (horizontal) and y axis (vertical) being two main polarization axes of PM fiber, α being variable, and $\theta = 25°$.

When θ is 25°, the pulse can be decomposed into two orthogonal polarization components which transmit in the fast axis and slow axis in a PM fiber. Two orthogonal components are mainly affected by GVM, self-phase modulation, and cross-phase modulation (XPM) in PM fiber. After propagating an enough distance the two orthogonal components walk off during pulse transmission due to the large difference in refractive index between fast and slow axes of PM fiber, which will weaken the XPM effect. To solve the problem, a Faraday rotator and an end mirror are used to rotate polarization state of the pulses by 90° for automatically compensating for the GVM introduced by the fiber birefringence. Therefore, PBS, PM fiber, Faraday rotator, HWP, and end mirror jointly act as ASA.

3. Experimental results

Mode locking can be obtained with different cavity lengths and the characteristics of the laser from PBS are easily detected. Figure 3(a) shows the plots of output power *versus* pump power at different cavity lengths. Because the fiber is relatively long and the dispersion is relatively large, the mode-locked pulse generates typically nanosecond pulses.[21] Figure 3(b) shows the spectra measured with an optical spectrum analyzer (YOKOGAWA AQ6370 C with a resolution of 0.2 nm) with different cavity lengths at pump power of 600 mW. The central wavelength of the laser with 23-m-long cavity and 38-m-long cavity are both 1034.8 nm, and the corresponding full width at half maximum (FWHM) of spectrum is 5.66 nm and 5.32 nm, respectively. The spectrum of the 99-m cavity is split into two parts, whose central wavelength is 1030.2 nm and 1039.8 nm with a separation of 9.6 nm.

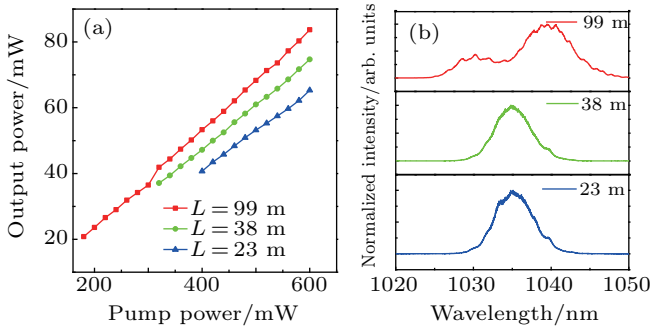


Fig. 3. Characteristics of lasers with three cavity lengths: (a) plots of output power *versus* pump power, and (b) spectra of lasers.

Figures 4(a)–4(c) show temporal pulse shapes sampled by a 4-GHz sampling oscilloscope (Tektronix, DPO 70604C) equipped with a high-speed 15-GHz photodetector (Newport, 818-BB-35F) with different cavity lengths. When the cavity length is shorter than 23 m, the mode locking cannot be started; while the mode-locking is unstable when the cavity length is longer than 99 m. The pulse will split when the pump power exceeds 300 mW at a cavity length of 99 m. The maximum output power is 83.7 mW at the pump power of 600 mW when the cavity length is 99 m, but the pulse

will split into three sub-pulses, which is primarily attributed to the increased nonlinear effect of the fiber with the increase of the pulse energy.[22,23] Therefore, the maximum pulse energy obtained is calculated to be 26.9 nJ with the cavity length of 38 m and the pump power of 600 mW, and the corresponding output power and the repetition frequency are 73.9 mW and 2.75 MHz, respectively. By comparing the performances of the lasers with different cavity lengths, it is noticeable that the pulse width, pulse energy, and output power increase with the cavity length and pump power increasing. Further increasing the cavity length or pump power would lead the pulse to split in temporal profile or spectrum, which is similar to the results reported in Ref. [23]. Thus we speculate that the pulse splitting can be avoided by appropriately changing the transmission characteristics of ASA,[24] or by inserting a filter into the cavity.

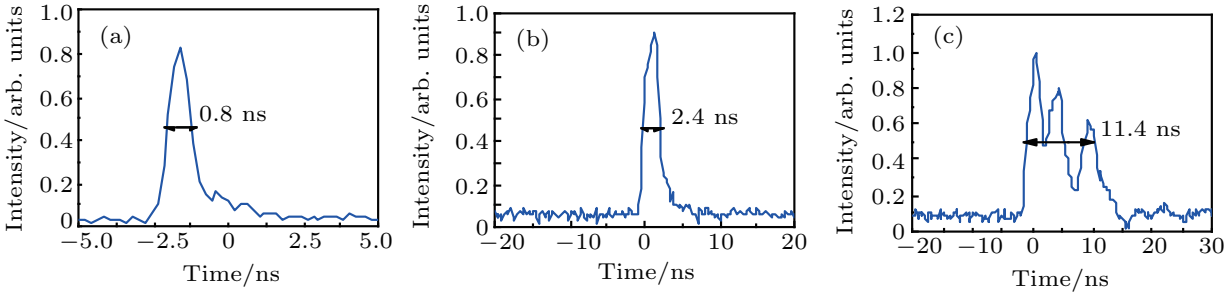


Fig. 4. Pulse's temporal profiles at cavity lengths of (a) 23 m, (b) 38 m, and (c) 99 m.

To investigate the long-term performance of the laser, the average output power is recorded over 12 h and the result is shown in Fig. 5. At the pump power of 600 mW and cavity length of 38 m, the average output power is 73.9 mW, and the standard deviation is 0.29 mW, with relative fluctuation being 0.39%. The mode locking will keep almost unaffected even we knock on the experimental table or touch the fiber, which demonstrates the good environmental stability of this laser.

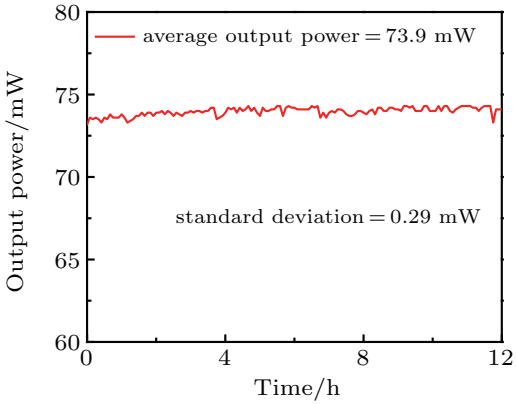


Fig. 5. Fluctuation of output power within 12 h with cavity length of 38 m at pump power of 600 mW.

Figures 6(a)–6(c) demonstrate the pulse trains of the mode locked pulses, and figures 6(d)–6(f) show the corresponding radio frequency (RF) spectra measured with a radio frequency spectrum analyzer (Agilent, Model: E4447A) at cavity length of 23 m, 38 m, and 99 m, respectively. It should be noted that there are two side lobes near the spike in Figs. 6(d)–6(f), but it is not obvious in Fig. 6(d). The frequency differences between the side lobes and the spikes are 0.013 MHz, 0.013 MHz, and 0.037 MHz, respectively. It is speculated that the synchronized jitter of each pulse gives rise to the side lobes.

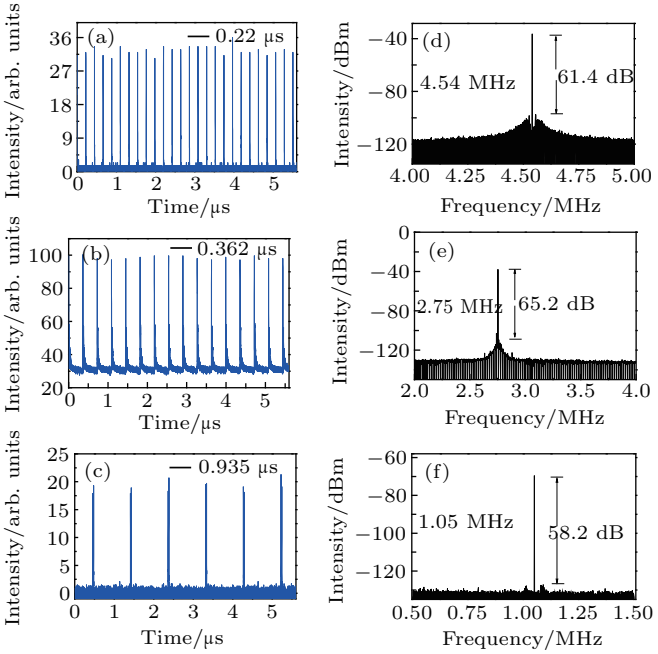


Fig. 6. Characteristics of mode-locking pulses: (a)–(c) pulse trains with cavity lengths of 23 m, 38 m, and 99 m respectively, and (d)–(f) corresponding RF spectra.

4. Theoretical analysis

The model of the ASA is shown in Fig. 2. The method we used is similar to those in Refs. [22,23]. Assume that the x axis (horizontal) and y axis (vertical) are two main polarization axes of the fiber, then the electric field of incident light can be decomposed into two components when it propagates alone the optical fiber. The matrix of amplitude envelope of the input light field can be expressed as[23]

$$\boldsymbol{A}_{\text{in}} = A_0 \begin{pmatrix} \cos(\theta) \\ \sin(\theta) \end{pmatrix}, \tag{1}$$

where A_0 is the amplitude envelope of the light field. The Jones transformation matrix for polarizer, HWP, and fiber (Kerr medium) can be expressed respectively as

$$\boldsymbol{J}_{\rm pol} = \frac{1}{2}\begin{pmatrix} 1+\cos(2\theta) & \sin(2\theta) \\ \sin(2\theta) & 1-\cos(2\theta) \end{pmatrix}, \tag{2}$$

$$\boldsymbol{J}_{\rm HWP} = \begin{pmatrix} -{\rm i}\cos(2\alpha) & -{\rm i}\sin(2\alpha) \\ -{\rm i}\sin(2\alpha) & {\rm i}\cos(2\alpha) \end{pmatrix}, \tag{3}$$

$$\boldsymbol{J}_{\rm kerr} = {\rm e}^{{\rm i}\psi}\begin{pmatrix} {\rm e}^{{\rm i}\Delta\psi} & 0 \\ 0 & 1 \end{pmatrix}, \tag{4}$$

where ψ and $\Delta\psi$ are the common phase shift and the differential phase shift, $\Delta\psi$ is expressed as

$$\Delta\psi = \Delta\psi_{\rm l} + \Delta\psi_{\rm nl}, \tag{5}$$

$$\Delta\psi_{\rm l} = \Delta\varphi + 2\pi\frac{L}{L_{\rm b}}, \tag{6}$$

$$\Delta\psi_{\rm nl} = \gamma\frac{L}{3}A_0^2(\cos(\theta)^2 - \sin(\theta)^2). \tag{7}$$

Here, $\Delta\psi_{\rm l}$ is the linear part of $\Delta\psi$, $\Delta\psi_{\rm nl}$ is the nonlinear part of $\Delta\psi$, $\Delta\phi$ is the cavity linear phase delay bias (CLPDB),[25] and L and $L_{\rm b}$ represent the length of the fiber and the beat length of the fiber, respectively. When the light is reflected back, the Jones transformation matrix of each device should be transformed into the transpose matrix of the original matrix.

Considering the half-wave loss, the Jones transformation matrix of the end mirror can be written as

$$\boldsymbol{J}_{\rm M} = \begin{pmatrix} -1 & 0 \\ 0 & -1 \end{pmatrix}. \tag{8}$$

Assuming that Faraday rotator makes the incident light polarization rotate an angle of Ω, the Jones transformation matrix can be written as

$$\boldsymbol{J}_{\rm FR} = \begin{pmatrix} \cos(\Omega) & \sin(\Omega) \\ -\sin(\Omega) & \cos(\Omega) \end{pmatrix}. \tag{9}$$

When the light propagates in the opposite direction throuth FR, Faraday rotator's Jones transformation matrix can be written as[26]

$$\boldsymbol{J}'_{\rm FR} = \boldsymbol{R}^{-1}\boldsymbol{J}^{\rm T}_{\rm FR}\boldsymbol{R}, \tag{10}$$

where $\boldsymbol{R}$ is the inverse coordinate transformation matrix and $\boldsymbol{R}^{-1}$ represents the coordinate transformation in the opposite direction to the laboratory frame. Therefore, the amplitude envelope of the light field passing through ASA can be expressed as

$$A_{\rm out} = \left|\boldsymbol{J}^{\rm T}_{\rm pol}\times\boldsymbol{J}^{\rm T}_{\rm kerr}\times\boldsymbol{J}'_{\rm FR}\times\boldsymbol{J}^{\rm T}_{\rm HWP}\times\boldsymbol{J}_{\rm M}\times\boldsymbol{J}_{\rm HWP}\right.$$
$$\left.\times\boldsymbol{J}_{\rm FR}\times\boldsymbol{J}_{\rm kerr}\times\boldsymbol{J}_{\rm pol}\times A_0\begin{pmatrix}\cos(\theta)\\ \sin(\theta)\end{pmatrix}\right|. \tag{11}$$

The transmission of the ASA can be expressed as

$$T = \frac{|A_{\rm out}|^2}{|A_{\rm in}|^2} = \frac{1}{2}\sin^2(2\theta)\left\{1-\cos\left[2\Delta\phi + 2\pi\frac{2L}{L_{\rm b}} - \gamma\frac{2L}{3}P\cos(\theta)\right]\right\}. \tag{12}$$

Figure 7(a) shows the plots of the simulated transmission *versus* input peak power at different cavity lengths. The cavity length has no influence on the maximum transmission of the ASA, but does affect the period of transmission. Increasing the cavity length can reduce the peak power corresponding to a maximum transmission, which means that the mode-locking threshold of the laser can be reduced. Figure 7(b) displays the plots the simulation of transmission *versus* input peak power at different values of θ. When the value of θ varies, the maximum transmission of the laser and the period of the transmission curve will significantly change correspondingly. At the same time, it is noteworthy in two aspects: (i) when the peak power is quite low, the transmissivity is close to zero, which is beneficial to improving the signal-to-noise ratio of the pulses after mode-locking, but the low-power transmission also inhibits the initial formation of pulse.[27] (ii) No item relative to HWP is seen in the above equation, *i.e.*, the simulation results do not seem to show that the HWP affect the transmission of the model.

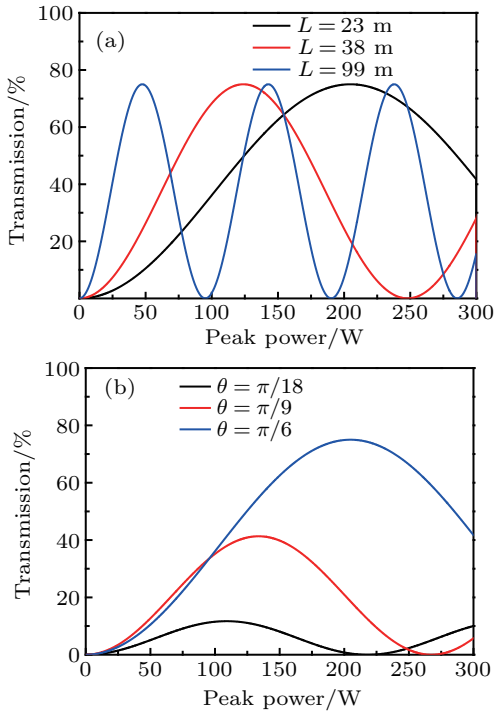


Fig. 7. (a) Plots of transmission *versus* peak power at different cavity lengths when $\theta = 30°$, and (b) plots of transmission *versus* peak power at different values of θ when cavity length is 23 m.

However, we find that when the HWP is not inserted between the Faraday rotator and the end mirror, or the surface of the HWP is perpendicular to the light path, the laser will not oscillate in experiment. However, when the HWP is inserted between the end mirror and the Faraday rotator in such a manner that the angle included between HWP and the axial line that connects the center of the end mirror and the center of the Faraday rotator is a Brewster angle, then the mode-locked

laser and continuous wave (CW) laser can be realized periodically. In order to explain the modulation of the laser output by the HWP in our experiment, it is necessary to rewrite the Jones transformation matrix of the HWP. When incident light passes through the HWP at a Brewster angle, the transmission of the component whose polarization state is parallel to the incident surface is $T_v = 1$, and the vertical component is[28]

$$T_{\rm h} = \frac{2n_0}{n_0^2+1}, \tag{13}$$

where n_0 is the refraction index of the ordinary wave. The Jones transformation matrix of the modified HWP is

$$\boldsymbol{J}_{\rm HWP} = \begin{pmatrix} -{\rm i}\cos(2\alpha) & -{\rm i}T_{\rm h}\sin(2\alpha) \\ -{\rm i}T_{\rm h}\sin(2\alpha) & {\rm i}T_{\rm h}^2\cos(2\alpha) \end{pmatrix}. \tag{14}$$

Therefore, the HWP brings about polarization-dependent loss. Figure 8 shows the characteristics of transmission with the loss of different polarization states taken into consideration. The maximum transmissivity can be affected by α. In the case of low input peak power (as shown by the red curve and the black curve in Fig. 8(b)), α has a periodic effect on the transmission at low peak power with a period of π. When α is an optimal value, the transmission will be improved, which is of benefit to the mode locking.

We theoretically discuss the effect of α on the transmission of ASA, and observe the output power and output state with respect to α in our experiment. Figure 9 shows the results. Figure 9(a) shows the plot of the simulated transmission of ASA, and figure 9(b) shows the experimental results of the average output power *versus* α. The red region represents the mode-locking state of the laser, while the green region represents the continuous wave state of the laser. As can be seen from Fig. 9(c), when the transmission of the ASA is near the maximum, the mode locking can be realized; when the transmission of the ASA is far from the maximum, the CW laser can be realized. The wave plate exerts influence within a period of $\pi/2$, which is well consistent with the experimental results. Therefore, we think, the polarization-dependent loss caused by the HWP affects the startup of the laser mode-locking state.

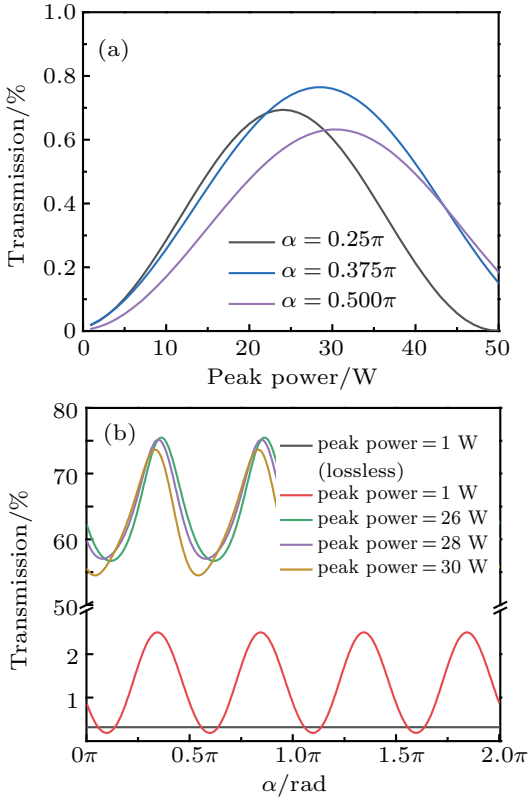


Fig. 8. Transmission characteristics of ASA: (a) plots of transmission *versus* input peak power at different values of α, and (b) plots of transmission *versus* α with different input peak power values with cavity length being 23 m.

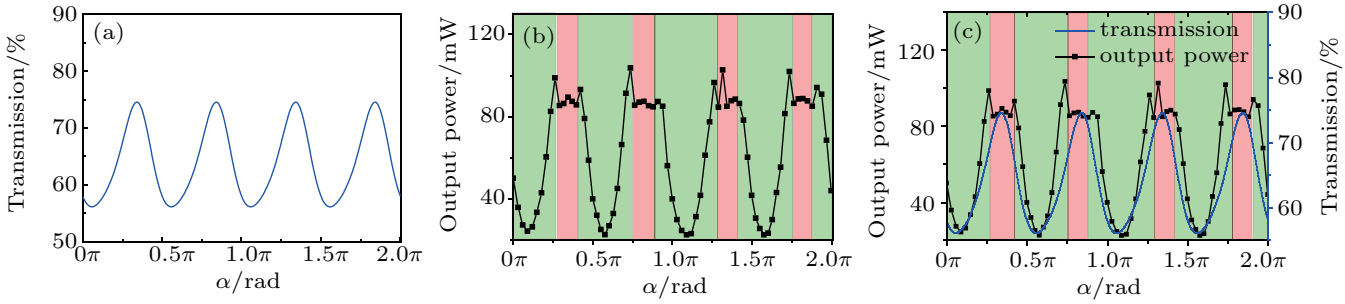


Fig. 9. The influence of α on output power: (a) simulated transmission of ASA; (b) experimental output power (the black line) with red region denoting laser operation in mode-locking and green region in CW state; (c) comparison between results in panels (a) and (b).

5. Conclusions

In this work, we demonstrate a linear cavity fiber laser based on PM NPE structure. A PBS is inserted into the cavity of a PM fiber laser to facilitate self-started mode-locking. By tuning the PBS to optimize the performance, self-started and long-term stable mode locking is achieved at different cavity lengths. The output power of 73.9 mW and pulse energy of 26.9 nJ are obtained at pump power of 600 mW. The output power is recorded for 12-h continuous operation and its standard deviation is 0.29 mW and the relative fluctuation is 0.39%, which demonstrates the good stability of the laser. If the power keeps increasing, the high-energy pulse may accumulate a large nonlinear phase shift. This distorts the pulse profile, and eventually the pulse will split. The influence of

the state of HWP arrangement on mode-locking of laser is discussed theoretically, obtaining a mode-locking range, which is in good agreement with the experimental result. Compared with the common PM fiber lasers, our design is simple and convenient, which does not require PM fiber angle-splicing nor precisely fiber length matching.

References

[1] Pan W W, Zhou J Q, Zhang L and Feng Y 2019 *Opt. Express* **27** 17905
[2] Hänsel W, Hoogland H, Giunta M, Schmid S, Steinmetz T, Doubek R, Mayer R, Dobner S, Cleff C, Fischer M and Holzwarth R 2017 *Appl. Phys. B* **123** 331
[3] Hao Q, Chen W H, Yang K W, Zhu X Y, Zhang Q X and Zeng H P 2016 *IEEE Photon. Technol. Lett.* **28** 87
[4] Zhang L, Zhou J Q, Wang Z K, Gu X J and Feng Y 2014 *IEEE Photon. Technol. Lett.* **26** 1314
[5] Sobon G, Sotor J and Abramski K M 2012 *Laser Phys. Lett.* **9** 581
[6] Xu J, Wu S D, Liu J, Li Y P, Ren J, Yang Q H and Wang P 2014 *IEEE Photon. Tech. Lett.* **26** 346
[7] Meng K, Zhu L Q and Luo F 2017 *Chin. Phys. B.* **26** 014205
[8] Liu X M, Yao X K and Cui Y D 2018 *Phys. Rev. Lett.* **121** 023905
[9] Liu X M and Pang M 2019 *Laser & Photon. Rev.* **13** 1800333
[10] Jeong H, Choi S Y, Rotermund F, Lee K and Yeom D I 2016 *J. Lightwave Technol.* **34** 3503
[11] Sotor J, Sobon G, Jagiello J, Lipinska L and Abramski K M 2015 *J. Appl. Phys.* **117** 133103
[12] Shen X L, Li W X and Zeng H P 2014 *Appl. Phys. Lett.* **105** 101109
[13] Szczepanek J, Kardas T M, Radzewicz C and Stepanenko Y 2017 *Opt. Lett.* **42** 575
[14] Wang Y Z, Zhang L Q, Zhuo Z and Guo S Z 2016 *Appl. Opt.* **55** 5766
[15] Zhou L, Liu Y, Xie G H, Zhang W C, Zhu Z W, Ouyang C, Gu C L and Li W X 2019 *Appl. Phys. Express* **12** 052017
[16] Szczepanek J, Kardas T M, Radzewicz C and Stepanenko Y 2018 *Opt. Express* **2** 13590
[17] Zhou J Q, Pan W W, Gu X J, Zhang L and Feng Y 2018 *Opt. Express* **26** 4166
[18] Peng Z G, Cheng Z C, Bu X B, Hong C, Li H J, Shi Y H and Wang P 2018 *IEEE Photon. Technol. Lett.* **30** 2111
[19] Szczepancek J, Kardaś T M, Piechal B and Stepanenko Y 2019 *Conference on Lasers and Electro-Optics (CLEO)*, San Jose, CA, USA, 2019 pp. 1–2
[20] Zhu X 1994 *Appl. Opt.* **33** 3502
[21] Xia H, Li H, Wang Z, Chen Y, Zhang X, Tang X and Liu Y 2014 *Opt. Commun.* **330** 147
[22] Shang J, Lu X, Jiang T, Lu Y and Yu S 2018 *Opt. Lett.* **43** 3301
[23] Xu R Q, Song Y R, Dong Z K, Li K X and Tian J R 2017 *Appl. Opt.* **56** 1674
[24] Cheng Z C, Li H H and Wang P 2015 *Opt. Express* **23** 5972
[25] Zhao L M, Lu C, Tam H Y, Wai P K A and Tang D Y 2009 *Appl. Opt.* **48** 5131
[26] Tan J, Chen W M and Yu M F 2007 *Opto-Electron. Eng.* **34** 120
[27] Nielsen C K and Keiding S R 2007 *Opt. Lett.* **32** 1474
[28] Yang T, Jing H M and Liu D H 2006 *Journal of Beijing Normal University* (Natural Science) **42** 477